LAWRENCE
LIVERMORE
NATIONAL
LABORATORY

LLNL-JRNL-668007

Origins of optical absorption characteristics of Cu2+ complexes in solutions

S. R. Qiu, B. C. Wood, P. R. Ehrmann, S. G. Demos, P. E. Miller, K. I. Schaffers, T. I. Suratwala

March 4, 2015

Journal of American Chemical Society

Disclaimer

Origins of optical absorption characteristics of Cu^{2+} complexes in solutions

S.R. Qiu*, B.C. Wood, P.R. Ehrmann, S.G. Demos, P.E. Miller, K.I. Schaffers, T.I. Suratwala
Lawrence Livermore National Laboratory, 7000 East Avenue, Livermore, CA 94551, USA

R.K. Brow
Materials Science & Engineering, Missouri University of Science and Technology, Rolla, MO 65409, USA
*qiu2@llnl.gov

Abstract

Many transition metal complexes exhibit infrared or visible optical absorption arising from *d-d* transitions that is the key to functionality in technological applications and biological processes. The observed spectral characteristics of the absorption spectra depend on several underlying physical parameters whose relative contributions are still not fully understood. Although conventional arguments based on ligand-field theory can be invoked to rationalize the absorption peak energy, they cannot describe the detailed features of the observed spectral profile such as the spectral width and shape, or unexpected correlations between the oscillator strength and absorption peak position. Here, we combine experimental observations with first-principles simulations to investigate origins of the absorption spectral profile in model systems of aqueous Cu^{2+} ions with Cl^-, Br^-, NO_2^- and $CH_3CO_2^-$ ligands. The ligand identity and concentration, fine structure in the electronic *d*-orbitals of Cu^{2+}, complex geometry, and solvation environment are all found to play key roles in determining the spectral profile. Moreover, similar physiochemical origins of these factors lead to interesting and unexpected correlations in spectral features. The results provide important insights into the underlying mechanisms of the observed spectral features and offer a framework for advancing the ability of theoretical models to predict and interpret the behavior of such systems.

Introduction

Transition metal ion complexes form the basis of coordination chemistry,[1] and are key ingredients in various natural and synthetic systems of interest. For many complexes, a particularly useful aspect is their intrinsic optical absorption, which arises from the existence of partially filled *d* orbitals. For isolated ions, the five *d* orbitals are degenerate, but this degeneracy is removed when the ion is placed in a host environment. The rearrangement or the splitting of the energies of the *d* orbitals strongly depends on the coordination geometry and the chemical nature of the host material. The removal of the degeneracy also enables symmetry-forbidden *d-d* transitions, which are typically at energies corresponding to transitions in the visible (Vis) or near infrared (NIR).[2] Unfortunately, the exact relationship between the spectral profile and the local structural, chemical, and environmental factors that give rise to it is not always well understood, making proper interpretation of specific spectral features very challenging. Addressing these difficulties could in principle enable molecular engineering to obtain a desired optical absorption profile, accelerating the design and development of optical materials with tailored optical properties across a wide variety of applications.

A number of parameters need to be considered for describing the optical characteristics of transition-metal complexes, as well as for revealing their probable configuration in biological settings.[3] These include the peak position, intensity, and the spectral width of the absorption band. Ligand-field theory is often invoked to explain trends in the *d-d* separation arising from different chemical environments, which in turn determines the peak absorption wavelength according to the spectrochemical series.[4] However, it provides no direct information about the oscillator strength upon absorption or the spectral line width. Moreover, in practice the spectral profile is highly sensitive to perturbations within both the colorant complex and the surrounding environment (i.e., solvent),[4-6] which further alter the electronic states associated with the optical transitions (see schematic in Figure 1). The contributing physical properties are therefore convoluted and interdependent, making them difficult to isolate experimentally when extracting structure-property relationships directly from optical spectra.

In this work we present an integrated experimental and theoretical approach that transcends conventional ligand-field theory interpretations to explore the physiochemical origins of the optical absorption profile of aqueous Cu^{2+} complexes in the Vis-NIR range, where the *d-d* transitions are observed. The approach combines optical (Ultraviolet-Visible-Near Infrared, UV-Vis-NIR) spectroscopy with first-principles molecular dynamics (FPMD) and time-dependent density functional theory (TDDFT).[7] Cu^{2+} complexes are extremely important as industrial colorants,[8,9] and are crucial to the functionality of a variety of biological systems and processes.[3,10] As an added advantage, Cu^{2+} has only one half-filled electronic orbital ([Ar] $3d^9$). This simplifies the description because possible transitions between multi-reference spin states can be ignored; viz., a Tanabe-Sugano diagram needs not to be used.[11]

To examine the effect of ligand substitution on the spectral profile, four model ligands are investigated: Br^-, Cl^-, NO_2^-, and acetate (Ac^-), in addition to the aqua complex. Each is a small, monovalent ion complex that demonstrates monodentate coordination with dilute concentrations of Cu^{2+} ions.[12-14] This facilitates direct comparisons without introducing additional confounding factors related to steric- or charge-related differences. Based on the reported spectrochemical series[2,4] which establishes the order of ligand field strength for common ligands, Br^- and Cl^- are classified as weaker ligands than that of water, whereas Ac^- and NO_2^- are stronger ligands. It should be noted that the ligand strength does not refer to the strength of the Cu-ligand bond, but rather the effect of ligand substitution on the spectral features: weak ligand substitution (e.g., Br^- and Cl^-) leads to absorption centered at longer wavelengths (lower energies), whereas exchanging with strong ligands (e.g., Ac^- and NO_2^-) leads to absorption at shorter wavelengths (higher energies) with respect to the pure aqua complex.[2]

As shown below, the absorption spectral profile of the Cu^{2+}-ligand complexes cannot be explained by ligand-field theory alone, but rather reflect a number of factors related to the ligand identity and concentration, fine structure in the electronic states, complex geometry, and solvation environment. In several cases, interesting and unexpected correlations emerge, which are traceable to similar physiochemical origins in the spectral features.

Methods and Approaches

Preparation of Cu^{2+} aqueous solutions

Aqueous cupric salt solutions were prepared volumetrically from stock solutions made at 10 times the required molarity. Double distilled water was subsequently added to produce each solution to the desired molarity. Because perchlorate ions do not complex with metal ions in aqueous solution,[15] copper perchlorate dehydrate salt (Alfa Aesar) was used to produce a solution of Cu^{2+} aqua complex. A concentration of 0.01 M of Cu^{2+} was used to ensure spectral measurements would neither saturate nor null the detector on the spectrometer. High purity (99.98% purity) sodium salts (Sigma Aldrich, J. T Baker, and Alfa Aesar) were used to provide each of the four different displacement ligands, namely, Br^-, Cl^-, Ac^-, and NO_2^-. The ligand-to-Cu^{2+} concentration ratios used for Br^-, Cl^-, and NO_2^- were 1:1, 10:1, 100:1, and 500:1. For Ac^-, only the highest concentration ratio (500:1) was tested to avoid contamination by possible side reactions between the ligand and the background ClO_4^- ion, such as the formation of CO_2 due to redox chemistry.[16,17]

The solution ionic strength was fixed at 5M by mixing sodium perchlorate with sodium ligand salts of proper amount to ensure that high concentrations of copper ligand complexes were achieved.[12] To avoid the formation of polynuclear complexes, the ligand concentration was chosen to be either equal to or greater than that of the Cu^{2+} ions.[18] Sodium ions in solution do not form complexes and have no *d* electrons to introduce interfering spectral bands in the Vis-NIR range to the Cu^{2+} complexes. All chemicals utilized were reagent grade and were used as

received. No precipitation was observed in any of the solutions throughout the spectrometry measurements.

Optical absorption spectroscopy

The optical extinction coefficients of the Cu^{2+} salt solutions were determined from transmission measurements in the 200-1100 nm spectral range which were collected using a suitable spectrophotometer (Shimadzu model UV-1601 PC) with the solution placed in 1 cm quartz cuvettes. To minimize background and interference from water absorption in the NIR range, copper-free reference solutions were carefully prepared with identical chemical composition and ionic strength to those of the appropriate copper-containing test solutions. Transmission measurements were used to calculate the absorption coefficient of Cu^{2+} (α, cm^{-1}) at the wavelength of interest by utilizing the exponential form of Beer's law.[19,20] The molar extinction coefficient (ε, $cm^{-1}M^{-1}$) was subsequently computed following the relationship $\alpha = \varepsilon \cdot c$ where c is the Cu^{2+} concentration in solution with units of molarity (M).

Quantum chemistry simulations

Consideration of the full solvation environment is necessary for accurately reproducing the structural properties of the solvated Cu^{2+} complexes.[21] Accordingly, FPMD simulations of solvated Cu^{2+}-ligand complexes were performed within the Quantum-ESPRESSO package[22] using density functional theory (DFT) in the plane-wave pseudopotential approximation. Ultrasoft pseudopotentials[23] were used for all atoms (with cutoffs of 30 and 300 Ry for the plane-wave basis and charge density, respectively), based on the Perdew-Burke-Ernzerhof (PBE) exchange-correlation functional.[24] A time step of 8 a.u. and an effective mass of 500 a.u. were used, with hydrogen treated as deuterium to facilitate the larger time steps. The water was first equilibrated for 10 ps independently without Cu^{2+}, then for another 10 ps with Cu^{2+} added before adding any other ligands. Following ligand addition, another 5 ps of equilibration was performed for each complex before acquiring 40 ps of production run trajectories. All dynamics were run in the *NVT* ensemble at 380 K to correct for the diffusive properties of water at ambient temperatures with the PBE functional.[25] Periodic supercells were cubic, and contained the Cu^{2+} ion with 48 water molecules (substituted as necessary with ligands) at the experimental density.

DFT geometry relaxations and single-point calculations of isolated Cu^{2+} complexes were performed within the NWCHEM software package.[26] TDDFT[7] within the Tamm-Dancoff approximation[27] was used to obtain the optical excitation energies. Similar approaches have been shown to be successful in predicting optical spectra of other transition-metal complexes.[5,6,28] The Baer-Neuhauser-Lifshifts (BNL) range-separated hybrid functional was used,[29] which treats short-range interactions within DFT and uses a Hartree-Fock formalism for the long-range interactions to provide the correct long-range asymptotic behavior.[30] This choice was motivated by a desire to describe different possible types of localized and charge-transfer excitations within the transition-metal complexes. A range separation parameter of 0.3747 was

chosen by enforcing Koopmans' Theorem to fix the ionization potential to the highest Kohn-Sham eigenvalue of the Cu-aqua complex.[29] The COSMO model[31] was used to simulate a solvation environment for both the DFT and TDDFT calculations.[32]

An augmented cc-pVTZ basis was used for Cu atom, and an augmented cc-pVDZ basis for all other atoms (in the present work, these larger basis sets were found to be required for proper convergence of the excitations).[33] To prevent improper spin state contamination in the localized basis, the restricted Hartree-Fock calculations on the ligand and Cu atoms were ran separately with dummy point charges substituting the absent species, then the vectors were used to run unrestricted Hartree-Fock calculations on the full system. These vectors were then used as inputs to the DFT and TDDFT calculations. As discussed below, for computing the TDDFT transitions, some geometries were based on relaxations of ideal complexes, whereas others were taken directly from the FPMD simulation trajectories. As a general rule, the TDDFT calculations tend to systematically overestimate the oscillator strengths, as well as the ligand-induced spectral shifts. This may be attributed in part to the absence of an explicit solvent in the TDDFT configurations, which will tend to strengthen the ligand-induced distortion.

Computational schemes for investigating spectral contributions

In general, ligand substitution of the aqua complex occurs according to the following chemical equation:

$$\left[Cu\left(H_2O\right)_n\right]^{2+} + xL^- \rightarrow \left[CuL_x\left(H_2O\right)_{n-x}\right]^{2+} + xH_2O$$

where L represents the substituting ligand, x is the level of substitution (number of substituted water molecules), and n is the first-shell coordination number of Cu^{2+}. Based on this formalism, four different computational schemes have been introduced in order to successively probe possible individual contributions to the observed spectrum. The procedures for computing the spectral features within each scheme are outlined in detail below.

Chemical Identity (CI) scheme: For the *CI* scheme, a geometrically relaxed, five-fold coordinated aqua complex was first constructed, based on previous results[6,34-38] showing strong evidence from first-principles dynamics simulations and X-ray spectroscopy that five-fold coordination in an octahedral symmetry (i.e., pyramidal) is the most common configuration for this complex. Ligands were then substituted for the axial water molecules, and the geometry of each resulting complex was allowed to relax before computing the relevant TDDFT transition energies and oscillator strengths. Note that the *CI* scheme retains five-fold coordination upon ligand substitution, while no thermal/solvent broadening effects are included. The reported peak positions E_{avg} are based on an average of the four TDDFT transitions E_i weighted by their respective oscillator strengths f_i: $E_{avg} = \sum_{i=1}^{4} \frac{1}{4} f_i E_i$. The reported oscillator strengths f_{tot}

represent the sum over the partial oscillator strengths for each of the four transitions: $f_{tot} = \sum_{i=1}^{4} f_i$.

The Water Coordination (WC) scheme: For the *WC* scheme, TDDFT transition energies and oscillator strengths are first calculated for geometrically relaxed complexes with different coordination numbers n (n=3,4,5,6) and at each level of ligand substitution *x* (*x*=1,2,3,4). Note that for the Ac- ligand, *x*=3 and *x*=4 were found to be unstable; the same was true for all complexes with substitution levels $x > 4$. Next, for every fixed value of *x*, relative probabilities of n (p_n) were obtained by statistically sampling the FPMD frames of the solvated complexes. Values of p_n for each ligand and each value of *x* can be found in Table S1. The average coordination found here for the aqua complex is similar to but slightly lower than those reported by Pasquarello et al. and Blumberger el al.. [6,34] The difference reflects likely the higher simulation temperature used here. The reported peak positions E_{avg} are based on an average of the four TDDFT transitions $E_{i,n}$ for each *n*, weighted by their respective oscillator strengths $f_{i,n}$ and probabilities p_n: $E_{avg} = \sum_{n=3}^{6} \sum_{i=1}^{4} \frac{1}{4} f_{i,n} E_{i,n} p_n$. The total oscillator strength is given by $f_{tot} = \sum_{n=3}^{6} \sum_{i=1}^{4} f_{i,n} p_n$. The *WC* scheme goes beyond the *CI* scheme to account for variability in the ligand coordination, which has been shown to be relevant for Cu^{2+} in solution, [6,36] but includes no solvent/thermal broadening.

The Geometric Distortion (GD) scheme: For the *GD* scheme, 150 frames sampled every 200 fs were chosen from the production runs for each value of *x*. Configurations for the TDDFT calculations were extracted from the FPMD frames by considering all molecules with atoms within the first solvation shell (~ 3.1 Å) of the central copper atom. The reported peak positions E_{avg} are based on a time average of the four TDDFT transitions $E_{i,t}$, each of which is weighted by the corresponding $f_{i,t}$: $E_{avg} = \frac{1}{T} \sum_{t=1}^{T} \sum_{i=1}^{4} \frac{1}{4} f_{i,t} E_{i,t}$. Here the index *t* runs over the *T*=150 frames included in the average. The total oscillator strength is given by $f_{tot} = \frac{1}{T} \sum_{t=1}^{T} \sum_{i=1}^{4} f_{i,n}$. The *GD* scheme explicitly includes solvent/thermal broadening effects, and is similar to the methodology used by other groups to investigate the spectra of ions in solution. [5,6]

The Ensemble Average (EA) scheme: For the *EA* scheme, the *x*-dependent values of $E_{avg,x}^{GD}$ and $f_{tot,x}^{GD}$ from the *GD* scheme are ensemble averaged according to the relative probability p_x of each *x* (*x*=1,2,3,4) at a given experimental ligand concentration (1:1, 10:1, 100:1, or 500:1). Accordingly, E_{avg} and f_{tot} become $E_{avg} = \frac{1}{4} \sum_{x=1}^{4} p_x E_{avg,x}^{GD}$ and $f_{tot} = \frac{1}{4} \sum_{x=1}^{4} f_{tot,x}^{GD}$. The p_x are computed by relying on the stability constants derived from the spectroscopic studies of Refs. [12,39,40], following the procedure outlined in the Supplementary Information (Figure S1 and Table S1). Because experimental stability constants were only available for NO_2^-, Cl^-, and Br^-, only values for these ligands within the *EA* scheme are reported here.

Results

Figures 2 and 3 show the dependence of the optical absorption spectra in the 1.0-2.3 eV range (Vis-NIR) on ligand concentration for weak (Figure 2) and strong (Figure 3) ligands. Focusing first on the energy of maximum absorption within this range, it is observed that weak ligands (Br^- and Cl^-) lead to absorption at lower energies than that for the pure Cu^{2+} aqua ion (1.54 eV or 805 nm), whereas strong ligands (Ac^- and NO_2^-) lead to absorption at higher energies than for the pure Cu^{2+} aqua ion. In addition, the shifts are greatest for Br^- and NO_2^-, the weakest and strongest of the tested ligands, respectively. This is as expected based on the respective ligand-field strengths of the complex ligands[2]. However, there are other additional effects that are not directly attributable to ligand field theory. For instance, ligand substitution leads to significant increases in the absorption amplitude, for both strong and weak ligands. Moreover, there are strong concentration effects; e.g., as ligand concentration is increased, there is a greater shift in the absorption peak energy and a more significant increase in the absorption amplitude. Similar observations have been reported by Friedman et al. for Cu^{2+} complexes in acetone-water mixtures where the extinction coefficient increased as H_2O was replaced by acetone in the solution.[15] The absorption peaks also deviate from a purely Gaussian distribution by skewing their centers towards higher energies.

To better understand the origins of the experimental spectral profiles in Figures 2 and 3 and to define trends in the optical absorption behavior of the ligand complexes, certain key parameters of the spectral profile for each ligand and concentration are plotted in Figure 4. In particular, the peak position of the absorption profile in the 1.0-2.3 eV range representing the energy where the maximum molar extinction coefficient is observed (see Figure 1), the peak height representing the maximum value of the molar extinction coefficient, the estimated full width half maximum (FWHM) of the spectral profile and the integrated oscillator strength are extracted. For the Cu^{2+} aqua complex and all ligands at all tested concentrations, a clear relationship emerges between the peak position and its height (Figure 4a). The molar extinction coefficient is lowest for the aqua complex, and increases almost linearly with the shift in peak position regardless of the shift direction. Here, it should be noted that the peak position includes cumulative effects from both the individual ligand field strength and the concentration-dependent level of ligand substitution (these two effects will be discussed separately later). On the other hand, the peak width (FWHM) in Figure 4b changes very little with ligand strength or level of substitution (standard deviation of ~0.04 eV, compared to an average FWHM of ~0.66 eV). Because the FWHM is relatively constant, the oscillator strength in Figure 4c (determined by a Gaussian fit to the integrated area under the peak) mirrors the dependence of the peak height in Figure 4a.

The salient trends in the peak position, width, and oscillator strength displayed in Figure 4 merit a broader question as to what additional geometric, chemical, and electronic structural information lies hidden in the spectra of the ligand complexes. In addition to providing fundamental understanding, such information is crucial for guiding the proper interpretation of optical spectra and for constructing proper theoretical models that more closely mimic

experimental conditions. Accordingly, the results in Figures 2-4 are accompanied by a detailed first-principles approach based on different computational "schemes" that are introduced to probe potential contributors to the peak profile individually rather than collectively. By comparing the computational predictions to trends in the actual spectra, the dominant factors controlling each peak feature in Figure 4 can be assessed. The focus is on explaining the behavior of: the peak position, oscillator strength, width, and skew, as well as the observed relationships between them.

Four different individual "ingredients" were identified as potentially relevant for determining the spectral profile. A theoretical scheme was devised for investigating each individual ingredient successively, described in detail in the Methods section. The four ingredients include: 1) the distortion of the electronic orbitals due the chemical identity of the ligands ("*CI*" scheme); 2) the specific water coordination around the central Cu^{2+} ion for each level of ligand substitution ("*WC*" scheme); 3) the degree of geometric distortion within the complexes due to thermal and solvent effects ("*GD*" scheme); and 4) ensemble averaging of different levels of ligand substitution ("*EA*" scheme). The key spectral features predicted by each scheme are shown in Figure 5.

Within the simplest *CI* scheme (Figure 5a), which already contains the most basic elements of ligand-field theory, the ordering of the peak position for the four ligands matches the spectrochemical series, as expected. In addition, although higher levels of ligand substitution do not always give rise to stronger shifts in the peak energy in the *CI* scheme (e.g., Ac^-, single- vs. double-substituted Br^-, and the Cl^- series), the *qualitative* relationship between the level of ligand substitution *x* and the peak position for each of the four schemes is already evident (see inset of Figure 5a, as well as Figure S2). Using more accurate schemes (*WC,GD, EA*) systematically improves the predicted magnitudes of the spectral shift and refines the relationship between *x* and the peak position (Figure S2). The inclusion of solvent/thermal effects in the *GD* scheme (Figure 5c and Figure S2) significantly reduces the ligand-induced peak shift. By comparison, including configurational (*WC*) or ensemble averaging (*EA*) of different *n* and *x* has a much smaller impact.

Although the *CI* scheme largely predicts the peak position, the relationship between the oscillator strength and the peak position is not captured until solvent/thermal effects are taken into account in the *GD* scheme (Figure 5c). This is because the description of the oscillator strength in the *CI* and *WC* schemes is qualitatively incomplete, and fails to exhibit the expected dependence on *x* (Figure S3). The *GD* scheme (Figure 5c) substantially improves the description, especially for high ligand concentrations. The *EA* scheme (Figure 5d) reproduces the full qualitative dependence, particularly by completing the picture for the weaker ligands. The computed values of the oscillator strength depend very strongly on the calculation scheme, and are mainly enhanced once environmental (solvent/thermal) factors are included.

The peak width is derived from the spectral broadening, which has two primary origins: static broadening, due to the spread in the electronic levels; and dynamic broadening, due to thermal and solvent effects (see schematic in Figure 1). These two factors are explored in Figure 6, which is based on the *GD* scheme. The horizontal axis of Figure 6 shows the *d-d* transition energy associated with each of the four distinct *d* levels (Δ_1 through Δ_4 in Figure 1), statistically averaged over all dynamics frames. The spread (Δ_4-Δ_1) across the Δ_i transitions, which approximates the static electronic broadening of the peak, is reasonably consistent across all tested configurations (average = 0.52 eV +/- 0.14 eV; see Table S3 for a breakdown by ligand type). The vertical axis of Figure 6 shows the FWHM of the distribution Δ_i of transition energies from the configurations explored in the dynamics, with the four electronic transitions (see Figure 1) examined individually. It provides a measure of the dynamic broadening associated with each transition. This quantity is also quite consistent for all tested configurations and transitions (average = 0.68 +/- 0.14 eV), and is similar in magnitude to the static contribution. Highly coordinated NO_2^- exhibits the most static and dynamic broadening, but the range is nevertheless comparable. The results in Figure 6 also illustrate that Δ_i generally decreases with increasing average transition energy; in other words, transitions that are higher in energy tend to be sharper, whereas lower-energy transitions are broader. This turns out to be related to the skew shape of the observed spectra, discussed in detail below.

Discussion

By synthesizing the simulation results in Figures 5 and 6 and comparing with the experimental observations in Figure 4, the physics underlying the peak profile can be deduced and interpreted. The general trend of the peak position as a function of ligand identity can be readily rationalized in light of ligand field theory, consistent with the visibility of the trend even in schemes that neglect dynamical contributions. However, the trends in the oscillator strength, and their connection to the peak positions, depend on factors other than the field strength alone. For instance, both strong and weak ligands give similar trends in the oscillator strength (Figure 4c). This is best understood in terms of ligand-induced symmetry breaking. As new ligands displace one or more water molecules to form a new mixed metal-ligand complex, hybridization of the Cu^{2+} *d* electrons will perturb the electronic orbitals and reduce the symmetry. The lowered symmetry will lead to a higher probability of *d-d* transition and thus the amplification of the absorption, regardless of the specific bonding mechanism. Within this logic, the oscillator strengths of both strong and weak ligands should respond similarly to distortion of the central Cu^{2+} orbital symmetry, as we observe.

According to the results of Figure 5c and the corresponding concentration-dependent values in Figure S3, the trend in the oscillator strength begins to be predicted only when combining the ligand-induced orbital distortion with the full space of geometric distortions due to thermal and solvent effects. Averaging over multiple coordination complexes that are simultaneously present in the solution further improves the description. It is concluded that both ligand-induced (i.e., chemical) and thermal/solvent-induced (i.e., mechanical) distortions in the electronic structure

contribute to the oscillator strength in Figures 4a and 4c. These two factors can be considered to have static and dynamic origins, respectively. The presence of multiple coordination complexes with different levels of substitution in each solution may also be relevant, as suggested in Refs. [12-14], although only for intermediate ligand concentrations and to a much lesser extent.

Careful examination of Figure 5 (and Figures S2 and S3 in the Supplementary Information) also reveals that there is an intrinsic coupling between the static and dynamic origins discussed above. Examining the aqua complex, which includes no additional ligand-induced chemical (static) distortions, it is observed that thermal/solvent-induced (dynamic) distortions have only a minor effect on the peak energy, but a huge effect on the oscillator strength. This leads to the logical conclusion that *f* is more sensitive to thermal/solvent-induced distortions, whereas the energy is primarily predicted by chemically induced distortions. On the other hand, looking at ligand-substituted complexes, it is concluded that the *sensitivity* of the peak position to dynamical effects actually depends on the identity and concentration of the ligand: much larger dynamical effects on the peak position are observed for the strongest and weakest ligands, and for the highest ligand concentrations (Fig. 5c). In other words, the presence of dynamical fluctuations due to solvent/thermal effects tends to reduce the energy shift of the peak, while simultaneously increasing the oscillator strength. This can be understood in terms of the effect on the crystal field that splits the *d* levels according to the depiction in Figure 1. For complexes with octahedral symmetry, the largest splitting—and hence the highest peak shifts—will occur when the Cu^{2+} *d* orbitals are well aligned with the ligand electrons, which will be closest to the relaxed geometry where the bond angles approach 90°. Once dynamical effects are included, deviations will necessarily lead to configurations with reduced symmetry and thus diminish the crystal field splitting[2,4], thereby decreasing the peak shifts as seen in Figure 5.

On the other hand, the oscillator strength depends on the electronic distortion of the *d* orbitals, which can be enhanced either from chemical (i.e., ligand substitution) or geometric (i.e., thermal/solvent) perturbations to the symmetry. Consequently, its value tends to increase upon inclusion of dynamical effects (note that this same interpretation implies that the oscillator strength should increase with temperature, which is confirmed experimentally for the aqua complex in Fig. S4). Comparing Figs. 5a-b with 5c-d, the highest sensitivity to thermal/solvent effects is observed for complexes with the highest degrees of ligand substitution. These observations lead to the conclusion that the static (ligand-induced) and dynamic (thermal/solvent-induced) distortions are in fact coupled. It is speculated that the chemomechanical coupling between them is ultimately responsible for the relationship between the peak position and oscillator strength in Figure 4c.

The consistency of the spectral width across the tested complexes in Figure 4b is also somewhat surprising. However, this can be rationalized in light of the results of Figure 6. The simulations clearly indicate that both the electronic broadening from additional fine structure in the *d* orbitals (which is a static effect), and the thermal/solvent broadening (which is a dynamical effect), are largely consistent across all of our tested complexes. Since these two factors are the dominant

contributors to the overall spectral broadening behavior (quantified by the FWHM), the spectral width changes little with ligand identity or concentration.

The results of Figure 6 also explain why the spectral profiles of the absorption band shown in Figures 1 and 2 are not strictly Gaussian, but are skewed towards higher energies. This is because the thermal/solvent broadening is inhomogeneous, and decreases linearly with the transition energy of Δ_i. As a result, the lower-energy edge of the spectral profile is more broadened than the higher-energy spectral edge. This behavior can be related to the lower sensitivity of higher-energy transitions to local changes in geometry. In other words, within a given complex, the levels that are most perturbed electronically by the presence of the ligands are also the least sensitive to geometric factors. A demonstration of how the electronic and thermal/solvent broadening effects can combine to give rise to the experimentally observed peak shape of the aqua complex based on the four contributing transitions Δ_i is shown in Figure S5. Significantly, the slope of the relationship between the transition energy and its thermal broadening (Figure 6) is quite consistent for a given ligand type, regardless of the specific level of ligand substitution *x*. Even across the different ligand types, the variation of the slope among the ligand types is not especially large (+/- 0.14, compared to an average slope of -0.48 across all complexes); nevertheless, stronger and weaker ligands tend to generate shallower slopes in Fig. 6 (computed slopes for each ligand type can be found in Table S3). The universality of these relationships illustrates yet another example of implicit coupling between static (i.e., electronic) and dynamic (i.e., thermal/solvent) contributions to the peak shape. It should be pointed out that the calculated slope could be used to quantitatively refine future descriptions of spectral profiles associated with *d-d* transitions.

Conclusions

In conclusion, the absorption spectra obtained from four model Cu^{2+}-ligand complexes in solutions is combined with first-principles simulations to examine many of the key physical contributors to the spectral profile characteristics of the Vis-NIR absorption spectrum. Interestingly, it is observed that the peak position and oscillator strength are intrinsically coupled for all tested ligand complexes. This is attributed to a subtle yet important connection between ligand identity and the sensitivity of the spectral features to solvent and thermal distortions. The spectral width is surprisingly consistent across the tested complexes, which is a direct result of the fact that both the electronic and thermal/solvent broadening effects are independent of ligand identity and concentration. At the same time, the thermal/solvent broadening is found to depend linearly on the optical transition energy, which leads to inhomogeneous broadening behavior and has the nonobvious consequence of skewing the peak profile towards higher energies.

The presented results conclusively demonstrate that conventional interpretations based on ligand field theory alone are insufficient for capturing the full characteristics of the absorption profile. Moreover, qualitative correlations between various aspects of the profile emerge upon deeper consideration of the physiochemical origins of the spectrum. The current study suggests a

compelling route for rationally designing and experimentally tuning the spectral profile of *d-d* transitions in metal-ligand complexes. The insights can be applied to better interpret experimental spectra, to help design materials with tailored optical properties as well as to provide a meaningful template for improving the accuracy of theoretical spectroscopic predictions.

Acknowledgement

This work was performed in part under the auspices of the U.S. Department of Energy by Lawrence Livermore National Laboratory under Contract DE-AC52-07NA27344. R.K.B. would like to thank Dr. C. Bischoff (Missouri S&T) for interesting discussions. S.R.Q. would like to thank Dr. P.H. Zhao (LLNL) for very fruitful discussions. B.C.W. acknowledges helpful discussions with Dr. V. Lordi and Dr. T. Ogitsu (LLNL).

References

(1) Huheey, J. E.; Keiter, E. A.; Keiter, R. I. *Inorganic Chemistry, Principles of Structure and Reactivity*; Fourth Edition ed.; Addison-Wesley Publishing Company, 1993.

(2) Figgis, B. N.; Hitchman, M. A. *Ligand field theory and its applications*; Wiley-VCH, 2000.

(3) Dhaveethu, K.; Ramachandramoorthy, T.; Therunavukkarasu, K. *Asian J. Chem.* **2014**, *26*, 3089.

(4) Douglas, B. E.; McDaniel, D. H.; Alexander, J. J. *Concepts and Models of Inorganic Chemistry*; Third Edition ed.; Wiley: New York, 1994.

(5) Bernasconi, L.; Blumberger, J.; Sprik, M.; Vuilleumier, R. *J. Chem. Phys.* **2004**, *121*, 11885.

(6) Blumberger, J.; Bernasconi, L.; Tavernelli, I.; Vuilleumier, R.; Sprik, M. *Journal of the American Chemical Society* **2004**, *126*, 3928.

(7) Runge, E.; Gross, E. K. U. *Physical Review Letters* **1984**, *52*, 997.

(8) Weyl, W. A. *Coloured glasses*; Society of Glass Technology, 1951.

(9) Bamford, C. R. *Colour Generation and Control in Glass*; Elsevier Scient.Publ.Company, 1977.

(10) de Almeida, K. J.; Murugan, N. A.; Rinkevicius, Z.; Hugosson, H. W.; Vahtras, O.; Agren, H.; Cesar, A. *Physical Chemistry Chemical Physics* **2009**, *11*, 508.

(11) Sugano, S.; Tanabe, Y.; Kamimura, H. *Multiplets of transition-metal ions in crystals*; Academic Press: New York and London, 1970.

(12) Khan, M. A.; Schwing-Weill, M. J. *Bulletin de la Societe Chimique de France* **1977**, *5-6*, 399.

(13) Arnek, R.; Puigdomenech, I.; Valiente, M. *Acta Chem. Scand. A* **1982**, *36*, 15.

(14) Kossiakoff, A.; Sickman, D. V. *J Am Chem Soc* **1946**, *68*.

(15) Friedman, N. J.; Plane, R. A. *Inorganic Chemistry* **1963**, *2*, 11.

(16) Schilt, A. A. *Perchloric acid and perchlorates*; The G. Frederick Smith Chemical Company Columbus, OH, 1979.

(17) Cotton, F. A.; Wilkinson, G.; Murillo, C. A.; Bochmann, M. *ADVANCED INORGANIC CHEMISTRY, 6TH ED*; Wiley India Pvt. Limited, 2007.

(18) Khan, M. A.; Schwing-Weill, M. J. *Inorganic Chemistry* **1976**, *15*, 2202.

(19) Valeur, B. *Molecular Fluorescence: Principles and Applications*; Wiley-VCH Verlag GmbH: New York, 2001.

(20) Barrow, G. M. *Physical Chemistry*; McGraw-Hill: New York, 1973.

(21) Bryantsev, V. S.; Diallo, M. S.; Goddard, W. A. *J. Phys. Chem. A* **2009**, *113*, 9559.

(22) Giannozzi, P.; Baroni, S.; Bonini, N.; Calandra, M.; Car, R.; Cavazzoni, C.; Ceresoli, D.; Chiarotti, G. L.; Cococcioni, M.; Dabo, I.; Dal Corso, A.; de Gironcoli, S.; Fabris, S.; Fratesi, G.; Gebauer, R.; Gerstmann, U.; Gougoussis, C.; Kokalj, A.; Lazzeri, M.; Martin-Samos, L.; Marzari, N.; Mauri, F.; Mazzarello, R.; Paolini, S.; Pasquarello, A.; Paulatto, L.; Sbraccia, C.; Scandolo, S.; Sclauzero, G.; Seitsonen, A. P.; Smogunov, A.; Umari, P.; Wentzcovitch, R. M. *J. Phys.-Condes. Matter* **2009**, *21*.

(23) Vanderbilt, D. *Physical Review B* **1990**, *41*, 7892.

(24) Perdew, J. P.; Burke, K.; Ernzerhof, M. *Physical Review Letters* **1996**, *77*, 3865.

(25) Grossman, J. C.; Schwegler, E.; Draeger, E. W.; Gygi, F.; Galli, G. *J. Chem. Phys.* **2004**, *120*, 300.

(26) Valiev, M.; Bylaska, E. J.; Govind, N.; Kowalski, K.; Straatsma, T. P.; Van Dam, H. J. J.; Wang, D.; Nieplocha, J.; Apra, E.; Windus, T. L.; de Jong, W. *Comput. Phys. Commun.* **2010**, *181*, 1477.
(27) Hirata, S.; Head-Gordon, M. *Chemical Physics Letters* **1999**, *314*, 291.
(28) Adamo, C.; Barone, V. *Theor. Chem. Acc.* **2000**, *105*, 169.
(29) Livshits, E.; Baer, R. *Physical Chemistry Chemical Physics* **2007**, *9*, 2932.
(30) Kummel, S.; Kronik, L. *Reviews of Modern Physics* **2008**, *80*, 3.
(31) Klamt, A.; Schuurmann, G. *J. Chem. Soc.-Perkin Trans. 2* **1993**, 799.
(32) Tomasi, J.; Mennucci, B.; Cammi, R. *Chem. Rev.* **2005**, *105*, 2999.
(33) Dunning, T. H. *J. Chem. Phys.* **1989**, *90*, 1007.
(34) Pasquarello, A.; Petri, I.; Salmon, P. S.; Parisel, O.; Car, R.; Tóth, É.; Powell, D. H.; Fischer, H. E.; Helm, L.; Merbach, A. E. *Science* **2001**, *291*, 856.
(35) Frank, P.; Benfatto, M.; Hedman, B.; Hodgson, K. O. *Inorganic Chemistry* **2008**, *47*, 4126.
(36) Chaboy, J.; Munoz-Paez, A.; Merkling, P. J.; Marcos, E. S. *J. Chem. Phys.* **2006**, *124*.
(37) Liu, X. D.; Lu, X. C.; Meijer, E. J.; Wang, R. C. *Physical Chemistry Chemical Physics* **2010**, *12*, 10801.
(38) Amira, S.; Spangberg, D.; Hermansson, K. *Physical Chemistry Chemical Physics* **2005**, *7*, 2874.
(39) Bjerrum, J.; Skibsted, L. H. *Acta Chemica Scandinavica Series a-Physical and Inorganic Chemistry* **1977**, *31*, 673.
(40) Kossiakoff, A.; Sickman, D. V. *Journal of the American Chemical Society* **1946**, *68*, 442.

Figures

Figure 1: Schematic of dominant sources of fine splitting in the energies of Cu^{2+} *d* orbitals that contribute to the optical absorption spectrum of solvated Cu^{2+}- ligand complexes. The symbol Δ represents the energy split between the e_g and t_{2g} states in the conventional crystal field description; symbols Δ_1 to Δ_4 display the fine splitting of the *d* levels due to additional environmental pertubations. The resulting optical spectrum is shown schematically in the right-hand panel, with its profile defined by the peak position, peak height, and full width half maximum (FWHM).

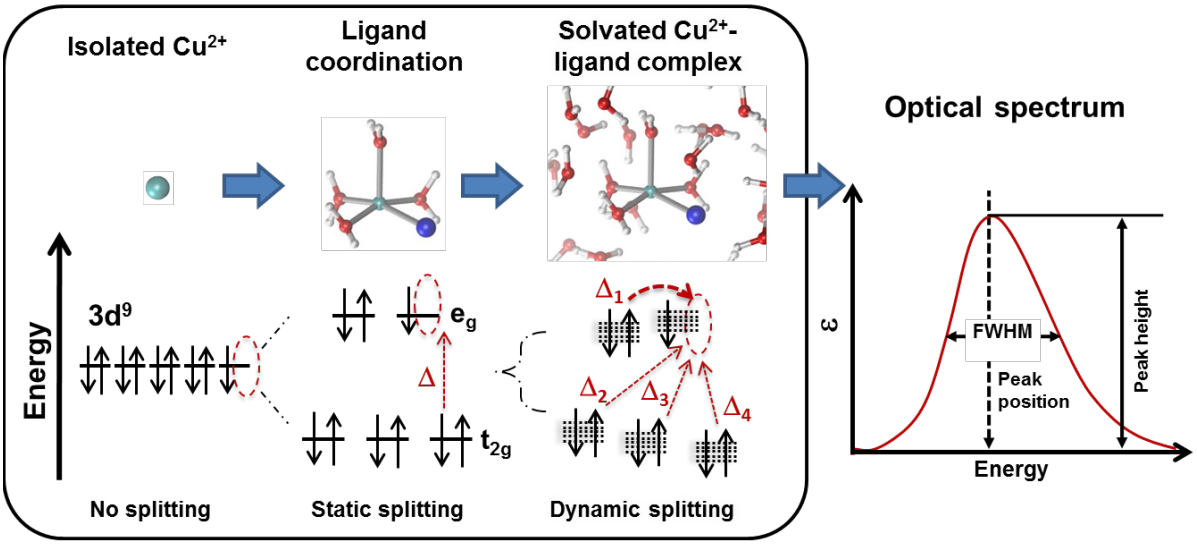

Figure 2: Optical absorption spectra of 0.01 M Cu^{2+} with different weak ligand-to-Cu^{2+} concentration ratios in the Vis-NIR range; (a) Br^- and (b) Cl^-. The vertical line segment indicates peak position at maximum absorption for each ligand concentration.

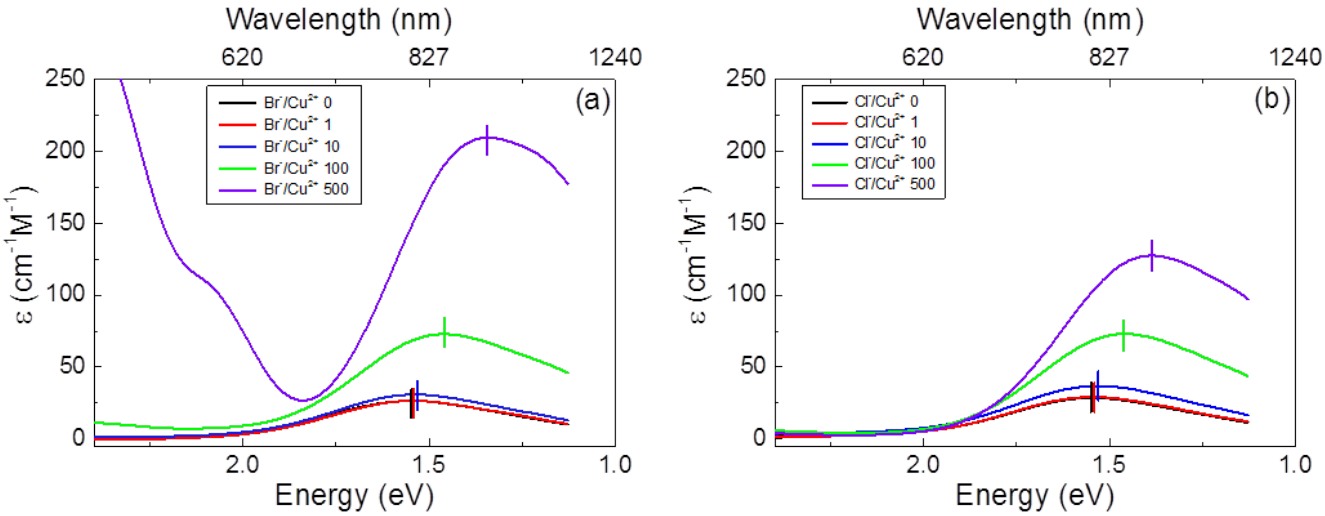

Figure 3: Optical absorption spectra of 0.01 M Cu^{2+} with different strong ligand to Cu^{2+} concentration ratios in the Vis-NIR range; (a) Ac^- and (b) NO_2^-. The vertical line segment indicates peak position at maximum absorption for each ligand concentration.

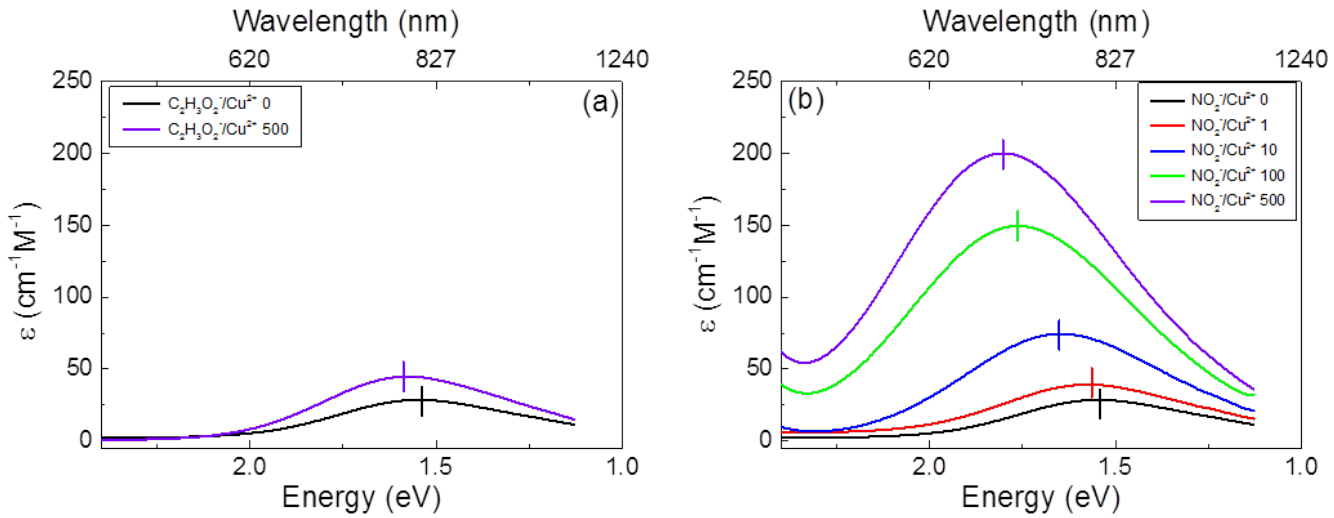

Figure 4: Correlation between the peak position of the Cu^{2+} absorption spectrum in the Vis-NIR range for all tested Cu^{2+}-ligand complexes and: (a) the absorption peak height, (b) the FWHM of the absorption spectrum and (c) the oscillator strength *f* estimated from (a) and (b). The arrows indicate trends with increased ligand concentration.

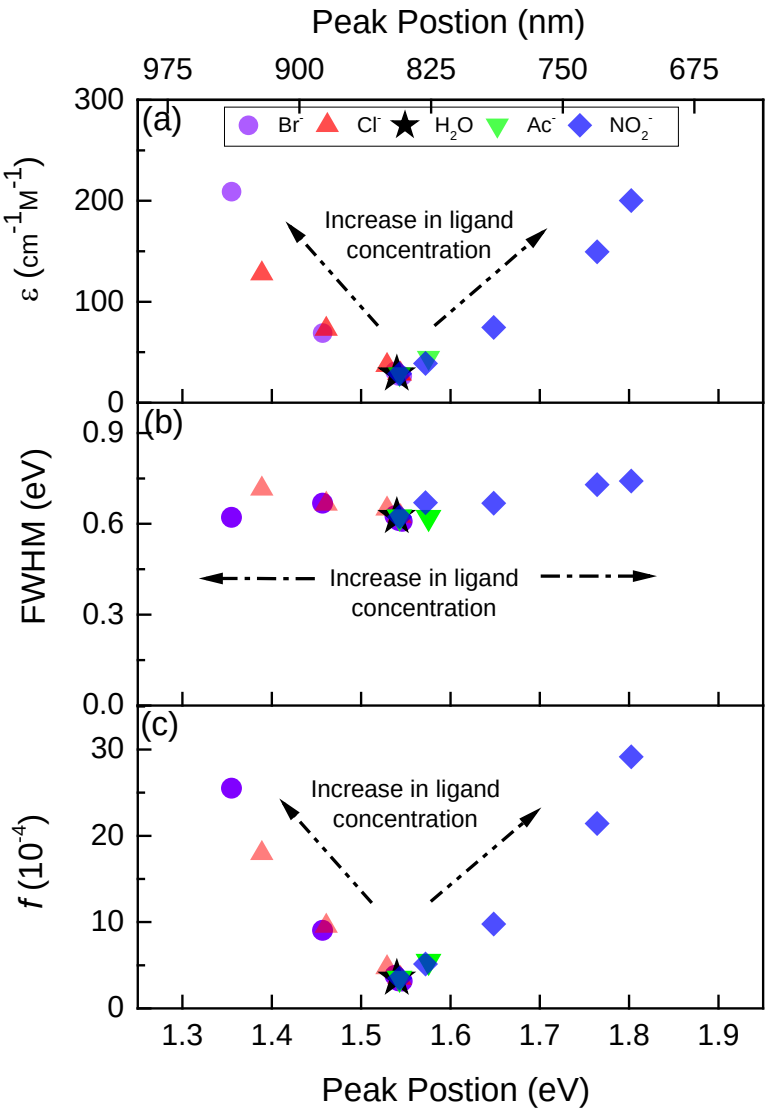

Figure 5: Oscillator strength versus peak position for all tested complexes, calculated within each of the four schemes described within the text: (a) CI, (b) WC, (c) GD, and (d) EA (note the differences in scale). The inset in (a) shows the dependence of peak position on ligand substitution *x* for the CI scheme.

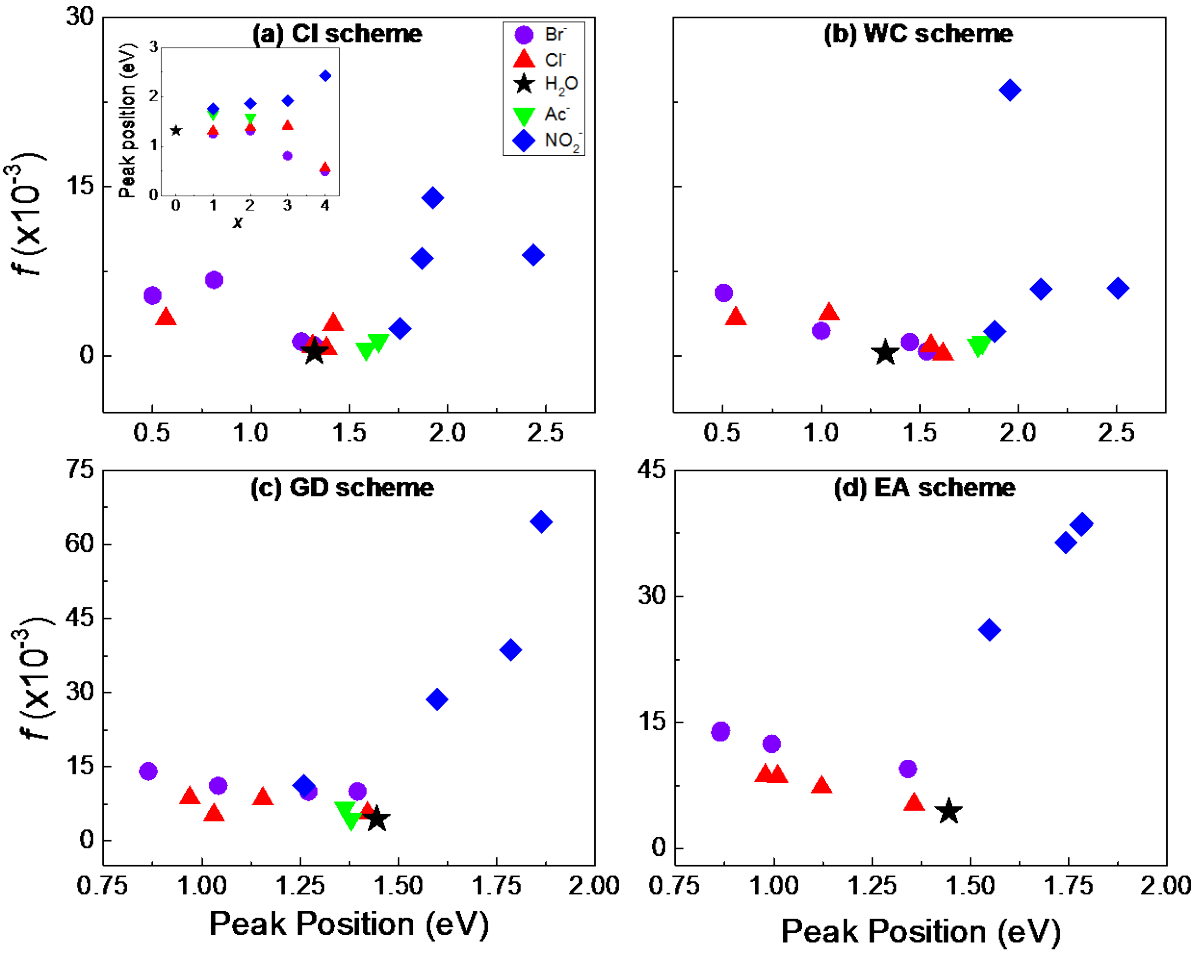

Figure 6: FWHM of Gaussian fit to computed distributions of Δ_i, plotted against the average Δ_i transition energy from first-principles molecular dynamics frames within the GD scheme. Data represent simulations with (a) Br^-, (b) Cl^-, (c) Ac^-, and (d) NO_2^- at each level of ligand substitution *x*. Linear fits to each data set are shown.

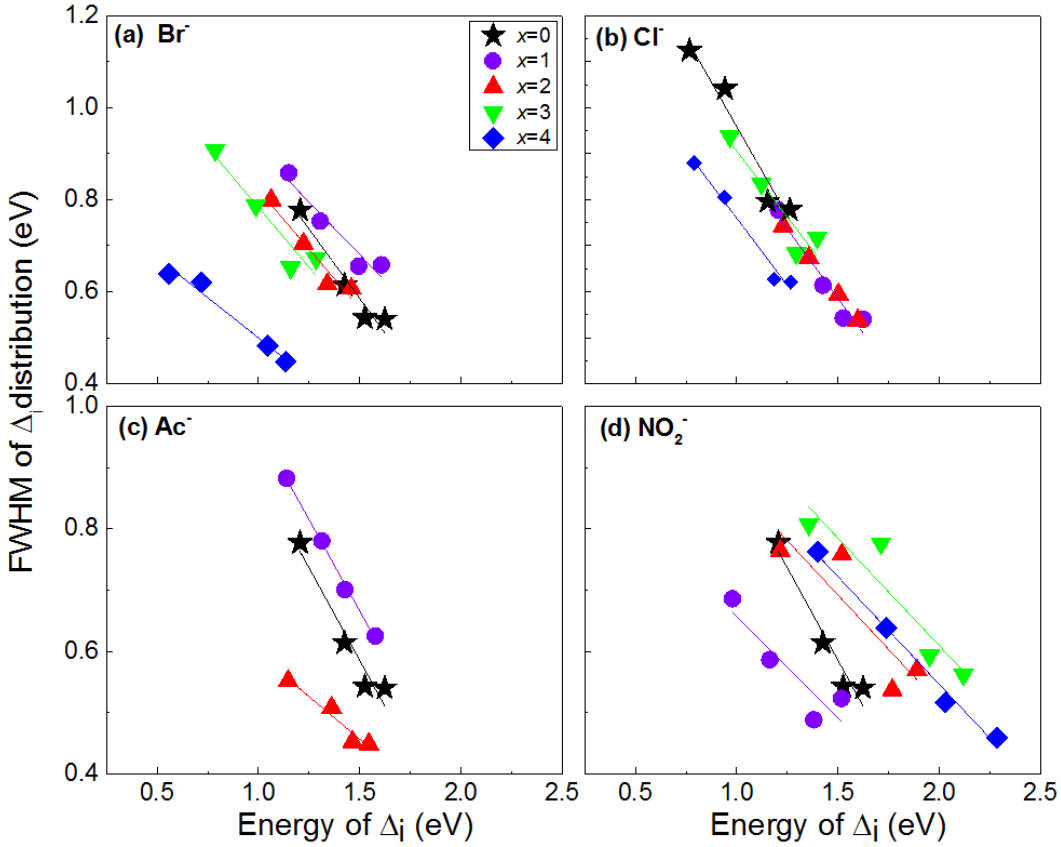

Supplementary Figures and Tables

Figure S1: Computed logarithmic fractional abundances for the Cu-ligand systems for three different ligands, based on published data[1-3]: (a) Br^- (*1*), (b) Cl^- (*2*), and (c) NO_2^- (*3*). The concentration dependence of the fractional abundance of each Cu-ligand complex species at equilibrium for an analytical Cu^{2+} concentration of 0.01 M is calcuated from the reported stability constants, based on the procedure outlined in Ref. [4]

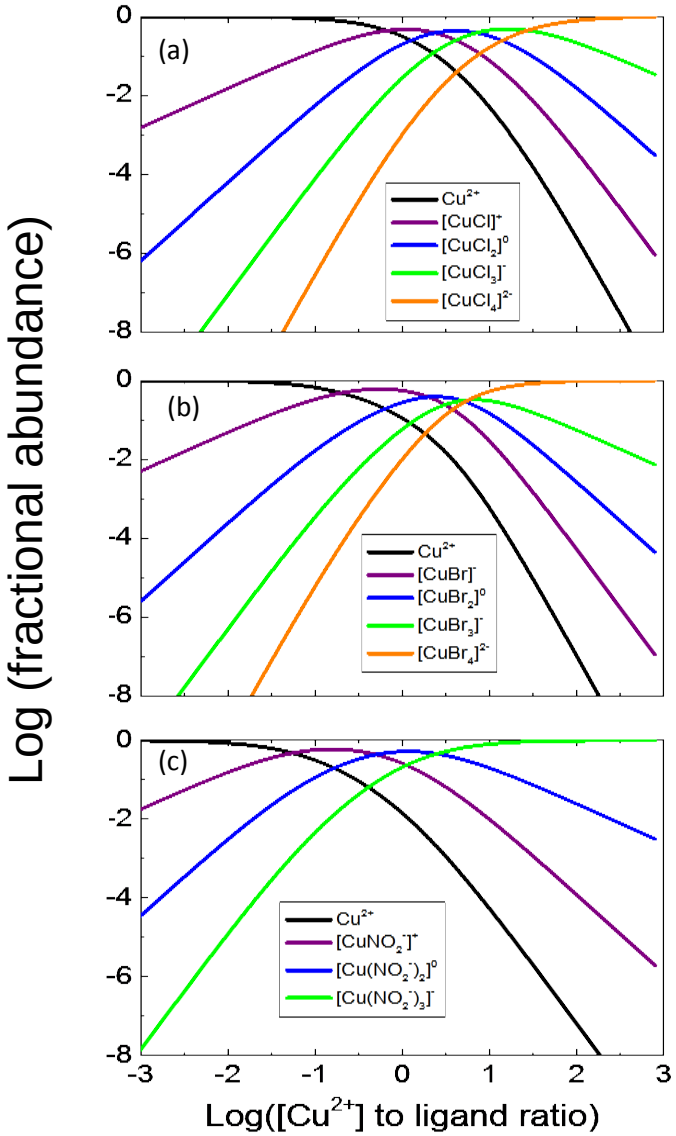

Figure S2: Peak position as a function of ligand substitution level *x*, calculated within the A) CI, B) WC, C) GD, and D) EA schemes described in the main text. The *x* values for the EA scheme are determined by weighting the fractional abundances in Figure S1 at each tested concentration (L^-:Cu^{2+} ratios = 1:1, 10:1, 100:1, 500:1).

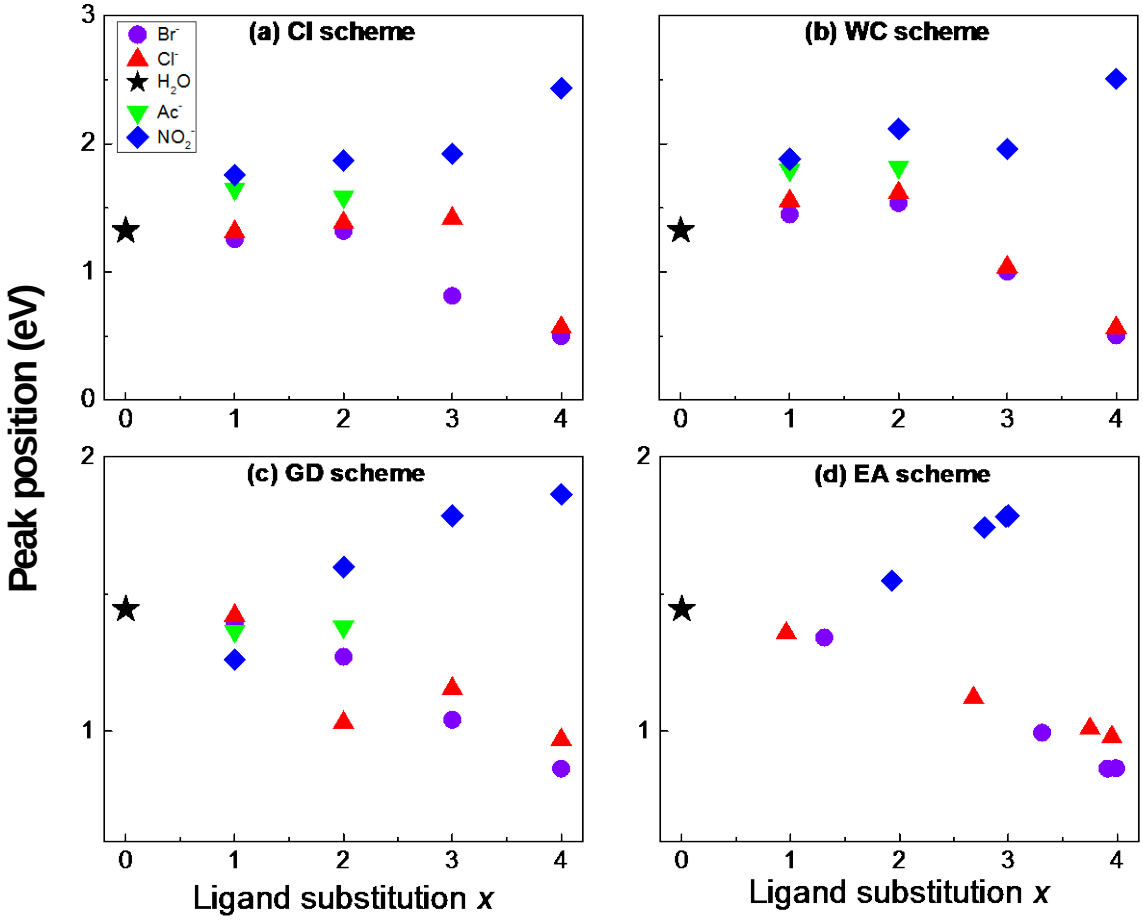

Figure S3: Oscillator strength as a function of ligand substitution level *x*, calculated within the (a) CI, (b) WC, (c) GD, and (d) EA schemes described in the main text. The *x* values for the EA scheme are determined by weighting the fractional abundances in Figure S1 at each tested concentration (L^-:Cu^{2+} ratios = 1:1, 10:1, 100:1, 500:1).

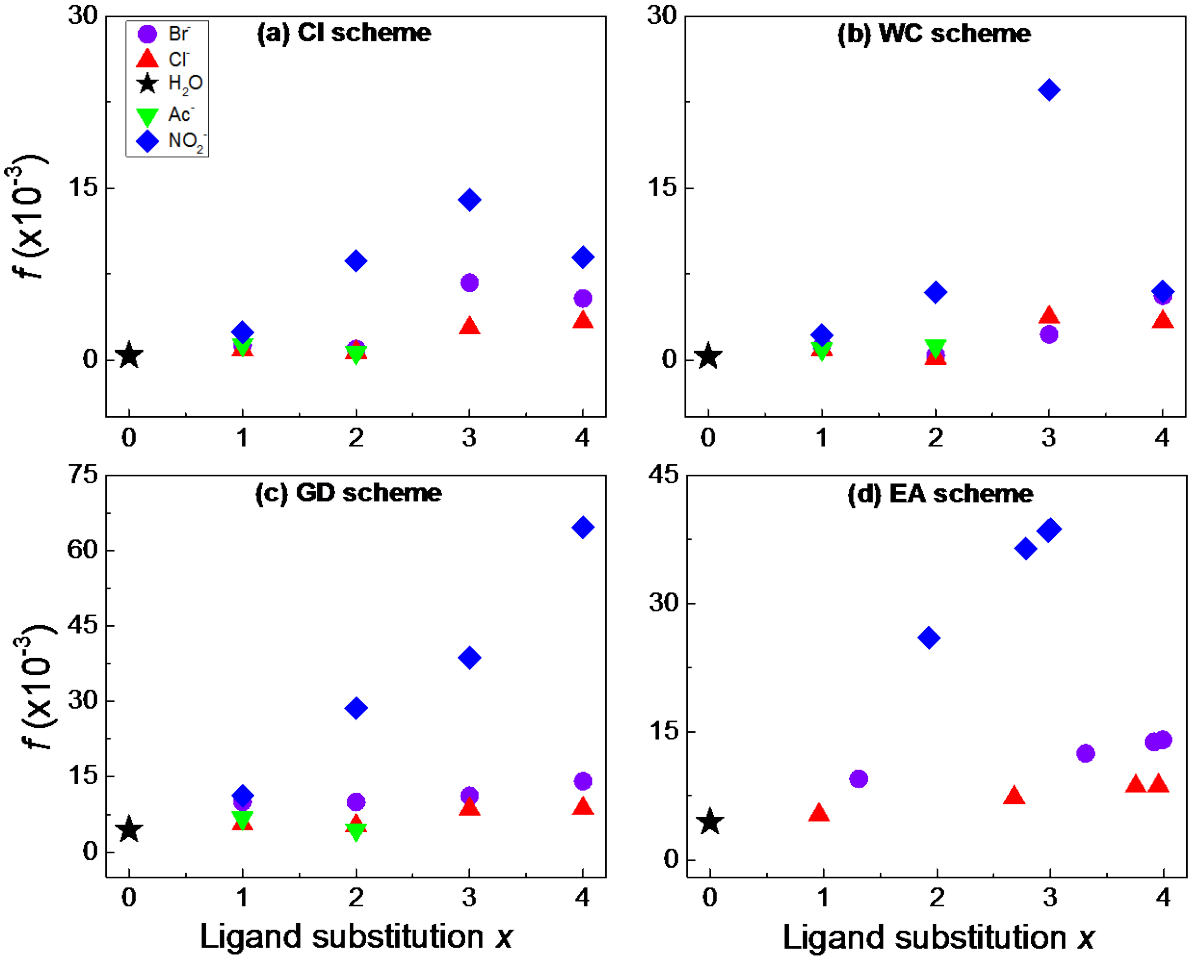

Figure S4: Optical absorption spectra of 0.01 M Cu^{2+} aqua solution collected at two different temperatures; (a) 25 °C and (b) 60 °C.

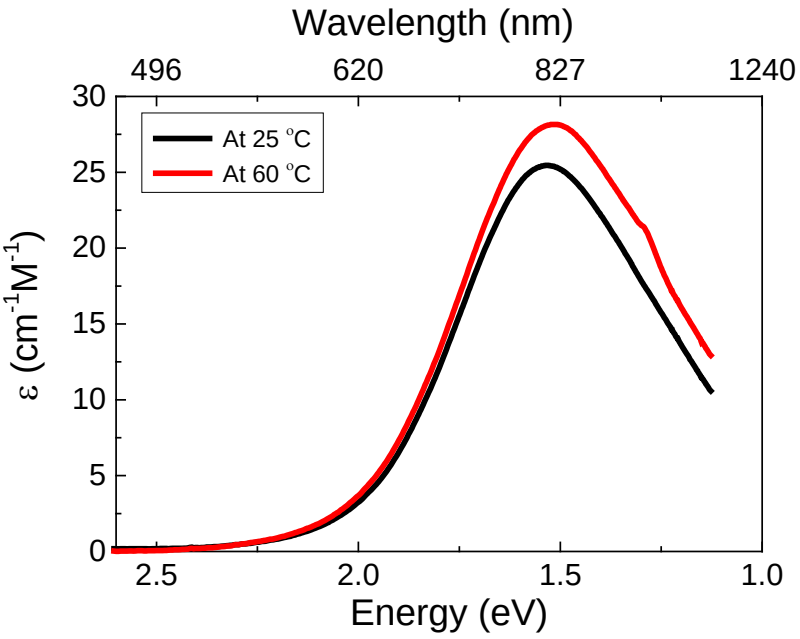

Figure S5: Computed peak profile for the Cu^{2+} aqua complex decomposed into the four contributing transitions Δ_i, including electronic and thermal/solvent broadening effects.

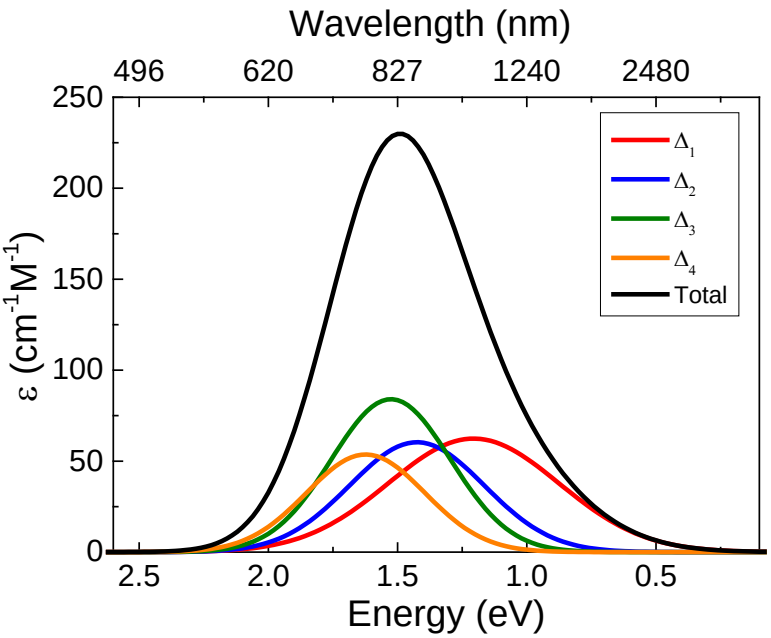

Table S1: Relative fractions p_n of first-shell coordinations n for Cu^{2+} at different levels of ligand substitution x, based on FPMD simulations.

Substituted ligand	**Level of substitution (x)**	**Fraction of n = 3**	**Fraction of n = 4**	**Fraction of n = 5**	**Fraction of n = 6**	**Average coordination number**
None (H_2O)	0	0	0.155	0.806	0.038	**4.88**
Br^-	1	0.001	0.437	0.55	0.012	**4.57**
	2	0.002	0.563	0.431	0.005	**4.44**
	3	0.097	0.84	0.062	0.002	**3.97**
	4	0.012	0.96	0.028	0	**4.02**
Cl^-	1	0.001	0.525	0.459	0.014	**4.49**
	2	0.013	0.733	0.222	0.03	**4.27**
	3	0.043	0.845	0.102	0.01	**4.08**
	4	0.001	0.908	0.088	0.004	**4.10**
Ac^-	1	0	0.464	0.524	0.011	**4.55**
	2	0.109	0.622	0.261	0.008	**4.17**
NO_2^-	1	0.017	0.724	0.237	0.022	**4.26**
	2	0	0.599	0.389	0.012	**4.41**
	3	0.004	0.486	0.491	0.019	**4.53**
	4	0	0.448	0.525	0.026	**4.58**

Table S2: Relative fractional abundances of different levels of ligand substitution *x* for each of the Cu^{2+}-ligand complexes as a function of the selected ligand concentration for (a) Br^-, (b) Cl^-, and (c) NO_2^-. Values are calculated from the analysis in Figure S1, based on data reported in Refs.[1-3]. The stability constants for the copper acetate complex were not available.

	[Ligand/[Cu^{2+}]	**0**	**1**	**10**	**100**	**500**
Br^-	*x = 0*	1	0.11	0	0	0
	x = 1	0	0.55	0.03	0	0
	x = 2	0	0.27	0.15	0	0
	x = 3	0	0.06	0.3	0.05	0.01
	x = 4	0	0.01	0.52	0.94	0.99
Cl^-	*x = 0*	1	0.31	0.01	0	0
	x = 1	0	0.47	0.08	0	0
	x = 2	0	0.2	0.32	0.02	0
	x = 3	0	0.03	0.44	0.21	0.05
	x = 4	0	0	0.16	0.77	0.95
NO_2^-	*x = 0*	0.98	0.01	0.00	0.00	0.00
	x = 1	0.02	0.26	0.01	0.00	0.00
	x = 2	0.00	0.52	0.20	0.02	0.00
	x = 3	0.00	0.21	0.79	0.98	1.00
	x = 4	0.00	0.00	0.00	0.00	0.00

Table S3: Average slopes (FWHM vs. Δ_i energy) and ranges (Δ_4 - Δ_1) in Figure 6 for each ligand species.

Substituted ligand	**Δ_4 - Δ_1(eV)**	**Fitted slope of FWHM vs. average energy**
None (H_2O)	0.42	-0.60
Br^-	0.48	-0.46
Cl^-	0.44	-0.62
Ac^-	0.42	-0.44
NO_2^-	0.72	-0.35

References

(1) Khan, M. A.; Schwing-Weill, M. J. *Bulletin de la Societe Chimique de France* **1977**, *5-6*, 399.

(2) Bjerrum, J.; Skibsted, L. H. *Acta Chemica Scandinavica Series a-Physical and Inorganic Chemistry* **1977**, *31*, 673.

(3) Kossiakoff, A.; Sickman, D. V. *Journal of the American Chemical Society* **1946**, *68*, 442.

(4) Freiser, H.; Fernando, Q. *Ionic Equilibria in Analytical Chemistry*; John Wiley & Sons, Inc: New York, 1963.